BCSIR

Facile synthesis of oriented zinc oxide seed layer for the hydrothermal growth of zinc oxide nanorods

S. F. U. Farhad[1]*, N. I. Tanvir[1], M. S. Bashar[2], M. S. Hossain[1], M. Sultana[2] and N. Khatun[1]

[1]*Solar Energy Conversion and Storage Research Section, Industrial Physics Division, BCSIR Labs, Dhaka 1205*

[2]*Institute of Fuel Research and Development (IFRD), Dhaka 1205, Bangladesh Council of Scientific and Industrial Research (BCSIR), Bangladesh*

Abstract

Oriented zine oxide (ZnO) seed layers were deposited by simple drop casting of zinc acetate dihydrate (ZAD) solution on glass substrates at room temperature followed by a post-heat treatment at 250 °C. X-ray diffraction (XRD) analyses revealed that ZAD solutions with concentration 0.0025 – 0.0100 M produced amorphous type thin films, whereas 0.0200 M ZAD solutions produced ZnO seed layers with a preferential c-axis texturing.The Scanning Electron Microscopy (SEM) analyses evident that the morphology of ZnO seed layer surface is compact and coherently carpets the underlying glass substrate. ZnO nanorods were then grown by hydrothermal method atop the ZnO seeded and non-seeded substrates. The presence of ZnO seeding layers was found to be beneficial for growing ZnO NRs films vertically. The optical bandgap of ZnO seed and ZnO NR were estimated to be in the range of 3.40 – 3.95 eV and 3.20 – 3.25 eV respectively by using UV-VIS-NIR diffuse reflection spectroscopy. The room temperature photoluminescence analyses revealed that nanostructured ZnO films exhibit a sharp near-band-edge luminescence peak at ~380 nm consistent with the estimated optical band gap and the ZnO nanorod arrays are notably free from defect-related green-yellow emission peaks.

Introduction

Zinc Oxide (ZnO) is one of the most studied semiconducting metal oxides with a wide direct bandgap of 3.37eV and a large exciton binding energy of 60 meV at room temperature. These intriguing properties together with wide range of functionalities (Ashfold *et al.,* 2007; Baruah and Dutta, 2009; Muth *et al.,* 1999; Schmidt-Mende and MacManus-Driscoll, 2007) make ZnO material a potential candidate for a wide variety of applications in optoelectronic devices, such as transparent conducting electrodes (Hiramatsu *et al.,* 1998) for flat panel displays, light emitting diodes (LEDs) (Jeong *et al.,* 2015; Sarangi *et al.,* 2017), solar cells (Nayeri *et al.,* 2013; Xu *et al.,* 2014), gas sensors (Kumar *et al.,* 2017), photodiode (Zhang *et al.,* 2014) and room temperature lasing (Chen *et al.,* 2000; Huang *et al.,* 2001) etc. In general, ZnO crystallizes in the thermodynamically stable, hexagonal wurtzite structure. Further, being a member of oxide family, ZnO is chemically stable and mechanically robust and can easily be grown by a number of deposition techniques (Islam *et al.,* 2011; Schmidt-Mende and MacManus-Driscoll, 2007) in a variety of low dimensional structures and morphologies such as nanoparticles (NPs), nanowires (NWs), nanorods (NRs), nanotubes (NTs), nanofibres (NFs) and nanobelts (NBs) etc. Among them, one dimensional (1D) ZnO nanostructures, such as NWs/NRs, with a predominant *c*-axis orientation gained remarkable attention because of its unique electrical, optical,

*Corresponding author e-mail: sf1878@my.bristol.ac.uk

mechanical, and chemical properties compared to its bulk counterpart (Greene *et al.,* 2005; Schmidt-Mende and MacManus-Driscoll, 2007; Vayssieres, 2003). Therefore, synthesis of ordered ZnO NRs growth along the *c*-axis normal is desirable, mainly for applications where crystallographic anisotropy is a prerequisite in order to attain efficient charge carrier transport and collection.

In recent years, *c*-axis textured ZnO seed layers have been grown by various deposition methods such as, Pulsed laser deposition (PLD) (Ashfold *et al.,* 2007), Magnetron sputtering (Yin *et al.,* 2014), spray pyrolysis (Peir *et al.,* 2006), Atomic laser deposition (Solís-Pomar *et al.,* 2011), sol-gel methods (Bao *et al.,* 1998), metal-organic chemical vapor deposition (MOCVD) (Kim *et al.,* 1992; Tan *et al.,* 2005) and thermal decomposition of drop-casted Zinc acetate solution (Greene *et al.,* 2005). Among them, the drop-casting technique is a simple, cheap and environment friendly synthesis technique which requires inexpensive equipment. Greene *et al.* (2005) reported the *c*-axis oriented ZnO nanocrystalline thin film on a variety of substrates by thermal decomposition of zinc acetate dehydrate (ZAD) solution in absolute ethanol in the range 200–350 ℃. They observed the highest *c*-axis texturing in the resulted ZnO thin film with an optimized 0.005M ZAD concentration and a subsequent decomposition temperature 350 ℃. Kim *et al.* (2005) reported sol-gel spin coating derived ZnO film with predominant *c*-axis orientation from ZAD precursor solution processed with various pre-heating temperatures (200–300 ℃) and a fixed annealed temperature 650 ℃ in the air for all samples. They observed the highest particle size for the film grown at 250 ℃ pre-heating temperature and a lower particle size and less *c*-axis oriented film for pre-heating temperatures 300 ℃ and above. They attributed the deterioration of *c*-axis texturing is due to the concurrent occurrence of solvent vaporization and abrupt thermal decomposition of ZAD. In this work, we report the synthesis and characterization of *c*-axis textured ZnO seeding layer at a low processing temperature 250 ℃ on soda lime glass (SLG) substrate. The post-heating temperature 250 ℃ was judicially selected for two reasons: first, to ensure decomposition of ZAD into ZS and its good adhesion on the substrate surface; and second, to avoid cracking of SLG substrate (glass softening temperature ~300 ℃) as well as deposited film atop the substrate surface. Therefore, the present study employs this *c*-axis textured ZnO thin film to provide vital nucleation center for subsequent growth of ZnO NRs arrays by a facile hydrothermal method. The structural, morphological, optical and photoluminescence properties of both ZnO seed and subsequent growth of ZnO NRs on seeded and non-seeded substrates were investigated and discussed.

Materials and methods

Chemical materials

Zinc acetate di-hydrate (Scharlau, purity~98%) and Absolute ethanol (Sigma-Aldrich, purity~98%) were used for ZnO seeding layer synthesis. Zinc nitrate hexahydrate (ZNH) (IndChem, >98%), Hexamethylenetetramine (HMT) (Scharlau, purity~98%) were used for hydrothermal growth of ZnO Nanorods (ZnO NRs) atop the seeded and non-seeded substrate. Deionized (DI) water (Resistivity~18 MΩ.cm) was used for making solutions where necessary and all chemicals were used without further purification in film deposition.

Preparation of ZnO seeding layer by drop casting

Prior to thin film deposition, soda lime glass(SLG) microscopy slide and fluorinated tin oxide (FTO) coated glass were cut into 2 cm × 1 cm strips and cleaned by sequential ultra-sonication in acetone, isopropanol and DI water (Resistivity~18 MΩ.cm) for 15 min followed by a hot air blown dry. In case of SLG substrates, toluene was also used prior to immerse in acetone step.For growing ZnO seed layer, firstly, Zinc acetate dihydrate (ZAD) with varying molar concentrations (0.0025 M – 0.020 M) dissolved in absolute ethanol and then 20 - 30 μL of this precursor solution was dropcast onto the pre-cleaned substrates and left for 10 seconds and then rinsed off with clean ethanol. This process was repeated for 20 times for increasing the layer thickness. The seeded substrates were then annealed at 250 ℃ for 1 hour in the air with a 5 ℃/min heating rate and allowed to cool naturally to the room temperature by switching the furnace off.

Preparation of ZnO Nanorods by Hydrothermal Method

ZnO NRs were deposited atop the bare as well as the ZnO seeded (0.02M ZAD) SLG and FTO substrates by hydrothermal method (Vayssieres, 2003). The reason for choosing two types of substrates was to investigate the effect of substrate surface into the resulting morphological features of the synthesized nanorods. 0.1M aqueous solutions of ZNH and HMT were prepared using DI water separately and then mixed together in a Schott bottle. One bare and one seeded substrate were tied next to each other onto a pre-cleaned microscopy glass slide using PTFE thread tape. This microscopy glass slide was immediately put into the solution mixture at a tilted angle by the bottle walls and with the substrates facing the bottom surface of the bottle. During the hydrothermal growth, this kind of substrate placing is expected to substantially preclude the ZnO aggregates formed in solution from dropping on the substrate surface. The complex solution was then heated slowly up to 90±2 ℃ in a thermostatically controlled oil bath over a period of 80

minutes. During this time, the appearance of the complex solution changed from clear to cloudy confirming the reaction taken into place. During the full deposition time, the reaction mixture in the Schott bottle was kept sealed and oil bath temperature was held at ~90 ^{0}C. After 1 hour, the substrates were removed from the solution and rinsed thoroughly with copious DI water and dried under a blow of hot air. The hydrothermally grown thin films were given to the same post-heat treatment as that of seeding layer (heated at 250 ^{0}C in the air for 1 hour) for removing any organic deposits from the bath solution.

Characterization techniques

The structural as well as phase identification measurements were carried out by a powder X-ray Diffractometer (PXRD) (EMMA, GBC scientific equipment) with a step size of 0.02 deg. using a Cu_K$_{\alpha1}$ (λ=1.54062Å) radiation source operated at 40kV and 40mA. The surface morphology was investigated by the Scanning Electron Microscope (SEM) (Hitachi S3400N). The optical transmittance and reflectance measurements of samples were made using a UV-VIS-NIR (Shimadzu 2600) spectrophotometer coupled with an integrating sphere. A custom made black mask with a ~8mm dia. hole at the center was used for ensuring a same illuminated area for all samples being investigated. Prior to optical measurements, the custom-made mask without any sample was used for baseline correction in case of the transmission data. In the case of reflection data, the BaSO$_4$ plate (came with the spectrophotometer) in conjunction with the custom made mask was used as the reflection standard. Photoluminescence spectra were recorded at room temperature (RT-PL) using a mini PL/Raman spectrometer (PHOTON SYSTEM) with a quasi-pulsed excitation source (HeAg 30 Deep UV laser, $\lambda_{ext} \approx 224$ nm). The scanning step size was set to 0.5 nm and number of pulses/step was set to 1 with energy 20µJ/pulse to avoid any possible photodegradation and/or laser induced local heating of the sample being investigated.

Results and discussion

ZnO seeds on SLG substrates

The structural properties of ZnO seed (ZS) films were examined by an X-ray diffractometer(XRD) in θ- 2θ (Bragg-Brentano geometry) coupled mode. Fig. 1(a) compares the XRD patterns of ZS as a function of ZAD solution concentration (0.0025 – 0.020 M) on SLG substrate, wherein X-ray diffractogram of ZnO powder (purity > 99.9%) is also included for the comparison

purposes. For pure ZnO powder, XRD pattern reveals diffraction peaks at $2\theta \approx 31.8^o$, 34.4^o, 36.2^o, 47.6^o which can be ascribed respectively to the $(10\bar{1}0)$, (0002), $(10\bar{1}1)$ and $(10\bar{1}2)$ reflection planes of hexagonal zincite phase as expected for a randomly oriented powder sample. Notice, the XRD patterns of ZS films (S1–S3) grown with lower ZAD concentrations (0.0025 –0.0100 M) do not exhibit any discernible Bragg peak (s) suggesting that they are mostly amorphous in nature (and they might be undetectable by the powder XRD setup conditions used due to the ultra-thinness of the deposited film). In contrast, the diffractogram of ZS film (S4) grown with 0.020M ZAD exhibit clearly distinguishable Bragg peaks with strong (0002) and a very week $(10\bar{1}1)$ reflection. The relative intensity of (0002) Bragg peak in the S4sample suggesting that ZnO seed layers were grown with a predominant *c*-axis texturing (Bao *et al.,* 1998; Kim *et al.,* 1992). The *c*-axis oriented ZnO seed layers are desirable for growing ZnO NRs vertically on the substrate surface (Yin *et al.,* 2014).

It is seen from the Fig. 1, the Bragg peak of S4 is conspicuously broad compared to those of ZnO powder indicating the nano-crystallinity of the ZnO seeds. The full-width half-maximum (FWHM) of (0002) Bragg peak of the S4 film was estimated to be ~0.927 deg. which is ~ 3 times larger than that of the ZnO powder (FWHM~ 0.295 deg.). Considering (0002) Bragg peak only, the average crystallite domain size (LC) of ZnO seed layer estimated to be ~9 nm compared to ~27 nm estimated for ZnO powder by using the Scherrer formula: $(\frac{180}{\pi})[(0.90 \times \lambda)/(FWHMcos\theta)]$ where, *FWHM* and θ are in degrees. Some other ımportant structural properties extracted from XRD data analyses are summarized in Table I for comparison with ZnO NRs samples (will be discussed later).

Fig.1(b). shows the SEM micrograph of S4 sample grown on SLG substrate.The morphology of ZnO seed layer surface is apparently compact and coherently carpets the underlying SLG substrate with dendrite-like networks (bright) throughout the area investigated. The magnified image of an area inside this networks are seen to be composed of spherically shaped grains of ~40 - 50 nm dia. (see inset of fig.1 (b). It is worth noting that seed layer surface is free from any micro-cracks and pinholes in reasonably large investigated area (~ 40 µm × 30µm), which is desirable for fabricating micrometer scale (opto) electronic devices. The surface morphology of S1–S3 ZS films (SEM image not shown here) on SLG substrate were found to be full of voids and discontinuous islands.
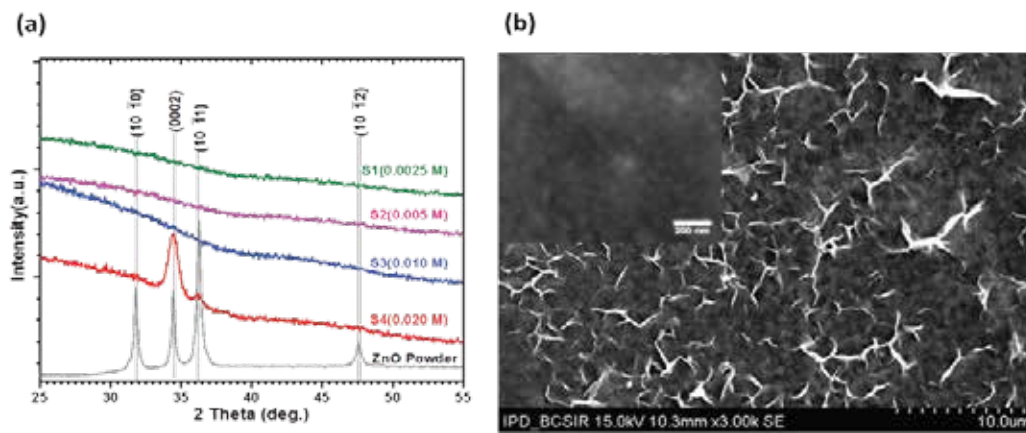
Fig. 1(a). XRD patterns (vertically offset for clarity) of ZnO thin films deposited at different ZAD solution concentrations on SLG substrates. The XRD pattern of ZnO powder (purity > 99.9 %) also is included for comparison purposes (b) The SEM micrograph of ZnO seed layer (S4) grown on SLG substrate, the inset displays a magnified image of the area inside dendrite-like network

Fig. 2(a) compares the normalized transmission spectra of S1–S4 samples including the blank SLG substrate (gray curve). The ZS films (S1–S3) grown with lower ZAD concentrations (0.0025 – 0.0100 M) exhibit~90% optical transparency but slightly lower than the blank SLG substrate near the absorption edge of the glass, presumably due to the ultra-thinness as well as amorphous nature of the ZS layer as mentioned earlier. In contrast, the transmission spectrum of ZS film (S4) grown with 0.020M ZAD exhibit ~80% optical transparency in the visible range on average and a distinguishable adsorption edge near $\lambda \approx 380$ nm which could be attributed to the ZnO film. There is an apparent tendency of decreasing optical transmission with increasing ZAD concentration which is depicted in the inset using optical data at three different wavelengths (360nm) (square), 400 nm (circle) and 460nm (triangle) around the absorption edge of ZnO. This observation means that there was indeed a layer formed in the case of S1-S3 film grown with lower ZAD solution concentration. To supplement this observation, diffuse reflection spectra were recorded for all samples to avoid optical contribution from underlying SLG substrate. Fig. 2(b) shows the variation of the bandgap of S1– S4 samples from the Tauc plot generated by using reflection data(shown in the Fig.2(b) inset) together with the so-called Kubelka-Munk function (F($R\infty$)) (Farhad, 2016):

$$F(R_\infty) = \frac{(1-R_\infty)^2}{2R_\infty} \quad (1)$$

where, $R\infty$ is the diffuse reflectance, and Tauc relation for direct band gap material can be written as (Farhad, 2016):
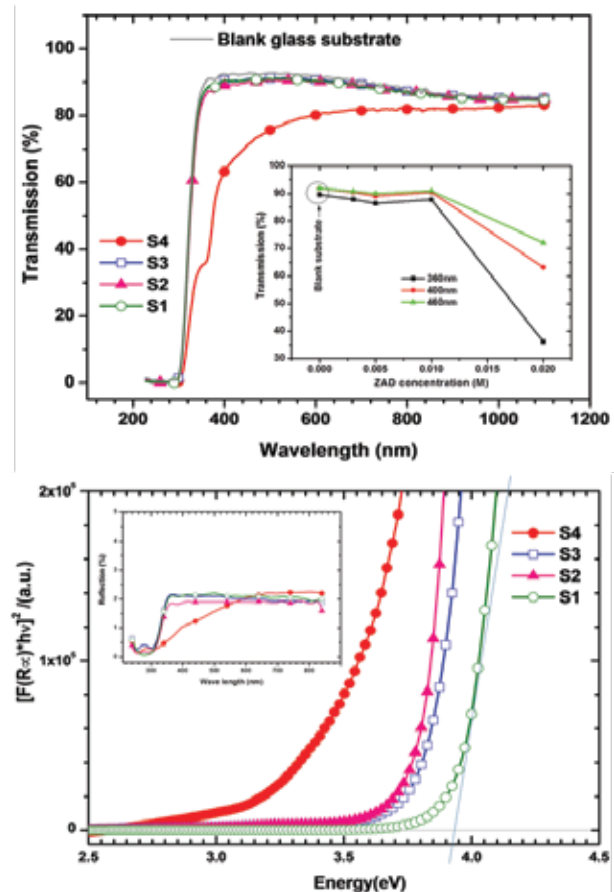

Fig. 2. Normalized transmission (top) and Tauc plot (bottom) for estimating band gap using diffuse reflection data (bottom inset) of ZnO thin films grown on glass substrate

$$\left(h\nu F(R_\infty)\right)^2 = A\left(h\nu - E_g\right) \qquad (2)$$

where E_g is the bandgap, is the proportionality constant, is the Planck's constant and is the frequency of the incident light. Therefore, by fitting a straight line to the curve of the plot vs one can obtain a bandgap value E_g in the -axis where the quantity must be zero. As can be seen from the Fig. 2(b), the bandgap of S4 film (E_g~3.45 eV) is much lower than those of S1–S3 films(E_g ~ 3.75 – 3.90 eV) suggesting that films grown with lower than 0.02M ZAD solution concentration are amorphous in nature, presumably composed of much lower size crystallites compared to S4 film (LC~9 nm). Recently, Tan *et al*. (Tan *et al.,* 2005) reported bandgap values in the range 3.13 – 4.06 eV for their MOCVD grown ZnO thin filmson quartz substrates and attributed the large blue shift (E_g ≥3.79 eV) of the bandgap is due to the amorphous nature of ZnO having crystallite size ~8 nm or lower. The amorphous thin films (S1–S3) grown with lower ZAD concentration will not be discussed in this report further.

ZnO NRs growth on seeded and non-seeded SLG and FTO substrates

Fig. 3 compares the XRD patterns of ZnO NRs grown on SLG and FTO substrates with and without ZS layer as mentioned in the legend of the corresponding curve.The diffractogram of pure ZnO powder and blank FTO substrate are also included in fig. 3 for reference (gray curves) and comparison purposes. The XRD pattern of the blank FTO also help us to rule out the peak shifting (if any) arises from the improper sample height adjustment on the 'XRD sample holder stub' and more importantly for identifying the substrate peak (s) in the deposited the film. It is worth mentioning here that all XRD patterns are normalized with respect to the highest intensity peak of the relevant samples and they are vertically offset for clarity. As can be seen, diffractogram of all deposited films regardless of substrate and seeding layer are dominated by the (0002) basal plane reflections of wurtzite ZnO phase suggesting that ZnO NRs produced by hydrothermal method were grown along the *c*-axis (Bao et al., 1998; J. S. Kim *et al.,* 1992; Yin *et al.,* 2014), presumably parallel to the substrate normal. However, a slight shift of the (0002) Bragg peak to the higher *2θ* angle can be distinguished for ZnO NR grown on seeded substrates compared to those of non-seeded substrates.The normalized intensity of (0002) peak was found to be always higher for ZnO NR grown on seeded substrate compared to the ZnO NR grown on non-seeded substrate, indicating that a seeded layer is indeed beneficial for controlling the *c*-axis texturing of the
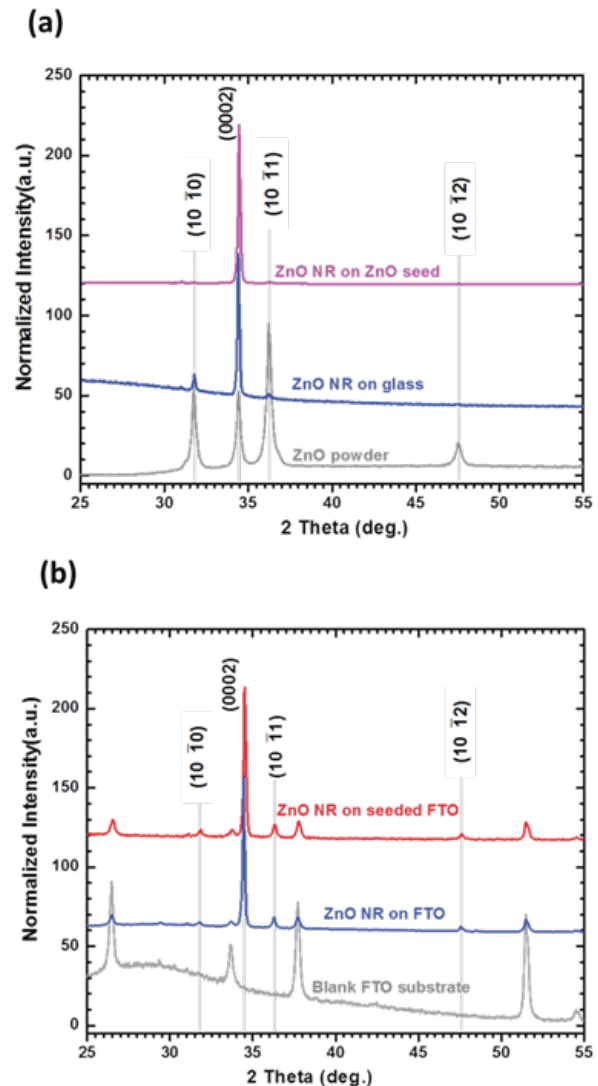

Fig. 3. Normalized XRD patterns (vertically offset for clarity) of ZnO nanorods grown with and without ZnO seed (S4) on (a) glass substrate and (b) FTO substrate by hydrothermal methods. The XRD pattern of ZnO powder (purity~99.9 %) and Blank FTO are also included in the respective panel for comparison purposes

hydrothermally grown ZnO NRs. Notice also that the Bragg reflections from non-polar faces of ZnO, for example, (10$\bar{1}$0) and (10$\bar{1}$1) are significantly suppressed for the sample ZnO NR/ZS/SLG compared to the ZnO NR/SLG (see fig. 3 (a)). A similar trend was also observed for samples grown on FTO substrate but the change is less conspicuous than those of the samples grown on SLG substrate, this is presumably due to less dense seed layer thereby fewer nucleation sites offered

by FTO as seen in the subsequent SEM micrograph analyses (discussed later).

The *c*-axis texturing in different films related to (0002) Bragg peak is denoted by TC (0002) and was estimated using following relation (Mekhnache *et al.,* 2011):

$$TC(0002) = N[\frac{I(0002)/I_0(0002)}{\sum_N I(hkil)/I_0(hkil)}] \qquad (3)$$

Where, *h, k, l,* and *i = -(h+k)* are the Miller indices for hcp crystal structure,   and   are the relative intensity of the deposited sample and standard sample with random orientation (ZnO powder) respectively and *N* is the number of Bragg reflections included in the analysis. The lattice parameter *a* and *c* as well as biaxial strain ($\varepsilon_{zz} = (c\text{-}c_0)/c_0$) and stress ($\sigma$) induced in the film were estimated using following relations (Mekhnache *et al.,* 2011):

$$\frac{1}{d_{hkl}^2} = \frac{4}{3}\left[\frac{h^2+hk+l^2}{a^2}\right] + \frac{l^2}{c^2} \qquad (4)$$

$$\sigma = -450 \times \varepsilon_{zz} \text{ GPa} \qquad (5)$$

Where, d_{hkl} is the interplaner spacing, *c* and c_0 are the lattice parameters for deposited films and strain-free standard sample (pure ZnO powder in our case) respectively. The structural parameters extracted from the XRD data analysis for all samples are listed in Table I.

As can be seen from the table I, the average crystallite domain size in all ZnO NRs samples is ~46±2 nm which about 5 times greater than that of ZnO seed/SLG and about 1.6 times greater than that of ZnO powder sample. Intriguingly, the estimated biaxial stress in ZnO seed/SLG and ZnO NR/SLG sample are compressive while it is tensile in ZnO NR grown on seeded SLG, FTO and seeded FTO substrates. Mekhnache *et al.* (2011) reported similar observations for their ZnO NR film grown on glass, ITO/glass and AZO/glass substrates by spray pyrolysis at T$_{sub}$= 350 ^{0}C and argued that the observed the change from compressive stress for ZnO NR/glass to tensile stress for ZnO NR/ITO/glass and ZnO NR/AZO/glass are due to the improvement of *c*-axis texturing. This is consistent with our results except for ZnO NR/SLG. Another possible reason might be that ZnO NR arrays grown on seeded substrates are more relaxed compared to those grown on non-seeded substrates. ZnO NR grown on SLG substrate was found to form a discontinuous film with lots of empty spaces and not all nanorods were grown parallel to substrate normal as evident from the subsequent SEM image. The surface morphology of ZnO NRs grown on seeded and non-seeded SLG and FTO substrates are illustrated in Fig. 4.

As can be seen from Fig. 4(a), only a few ZnO NRs were grown vertically on blank SLG substrate (non-seeded) and most of them lie in or on the substrate surface with few microns to few tens microns empty spaces among the nanorods (Length (L) ~2 - 10 μm and Dia. (D) ~ 0.5–1.0 μm). In the case of non-seeded FTO substrate, most of the substrate surface area was found to be covered by a very large number of horizontal rods, including a few areas with vertically grown thin nanorods (D~510 nm and L~2.24 μm) as seen in the inset of fig. 4(d). This is due to the fact that a clean FTO surface (see in the inset of fig. 4(f)) can offer more nucleation sites compared to blank SLG. However, their overall texturing is along the *c*-axis evident from the XRD pattern (see fig. 3). This observation suggests that strong (0002) reflection with high TC (0002) does not necessarily mean that they are grown parallel to the substrate normal. The horizontal NRs could presumably be precipitated from the nutrition solution during hydrothermal growth despite the thorough DI water rinsing employed after deposition.Sun *et al*. (2008) reported similar observation and argued that this is due to the enhancement of nucleation rate by the precipitation conditions.

Fig. 4(b). shows densely packed ZnO NRs arrays over a large area on oriented ZS layer (S4 film). The morphology of the underlying ZS layer (grown prior to the nanorod growth) is shown in fig. 4(c). In fig. 4(b), there are ZnO nanoflower-like structures atop the dense nanorod arrays, this is presumably a subsequent growth on nucleation sites available on ZnO NRs. ZnO nanoflower generally originates from common nucleation sites when the available ZnO seed densities are very low (Sun *et al.,* 2008). These ZnO NWs are relatively thin in dia. (D~ 30 − 200 nm and L~ 1− 2 μm) and their facets in the hexagonal cylinder are not conspicuous like those grown on ZS/FTO (see fig.4 (e)). Nanorods grown on seeded FTO possess well-defined hexagonal facets and they are seen to be the best vertically-oriented arrays among the samples investigated. In fig. 4(f), ZnO seed layer (labeled by SL, thickness~ 232 ± 34 nm) , FTO substrate (labeled by FTO, thickness~ 608 ± 22 nm), and vertically grown ZnO NRs (L~ 3.2 ± 0.1 μm) are evidently seen in the cross-sectional image of ZnO NR/ZS/FTO film. Clearly, fig. 4 (b, e, f) exemplify the beneficial effect of oriented ZS layer. Notice that in exact same conditions, seed layer promotes well-aligned nanorods arrays with 1.5 − 3 μm long, whereas, on non-seeded substrate rods grow up to 10 μm with random orientations.

The optical properties such as transmission, reflection as well as bandgap generally depend on crystallinity, surface morphology, and thickness of the film as well as surface roughness across the area of the sample being illuminated. Therefore careful efforts have been given during sampling

Table I. Structural properties obtained from X-ray diffractogram analysis

| Structural Parameters	ZnO Powder (Purity >99.99%)	ZnO seed (ZS)/SLG	ZnO NR/SLG	ZnO NR on ZS	ZnO NR on FTO	ZnO NR on ZS FTO
$2\Theta(0002)$ (deg.)	34.45	34.44	34.43	34.46	34.50	34.51
$d(0002)$ (nm)	0.26017	0.26024	0.26031	0.26009	0.25980	0.25973
a (nm)	0.31864	0.31873	0.31882	0.31855	0.31819	0.31810
c (nm)	0.52034	0.52048	0.52063	0.52019	0.51960	0.51946
FWHM (deg.)	0.295	0.927	0.172	0.184	0.175	0.182
Mean crystallite domain size (nm)	27.88	8.87	47.81	44.69	46.97	45.24
TC(0002)	Random	1.093	0.967	1.074	1.142	1.149
Strain(ε_{zz})$\times10^{-3}$	0.00	0.282	0.563	-0.281	-1.410	-1.690
Stress(GPa)	0.00	-0.12	-0.25	0.13	0.64	0.76
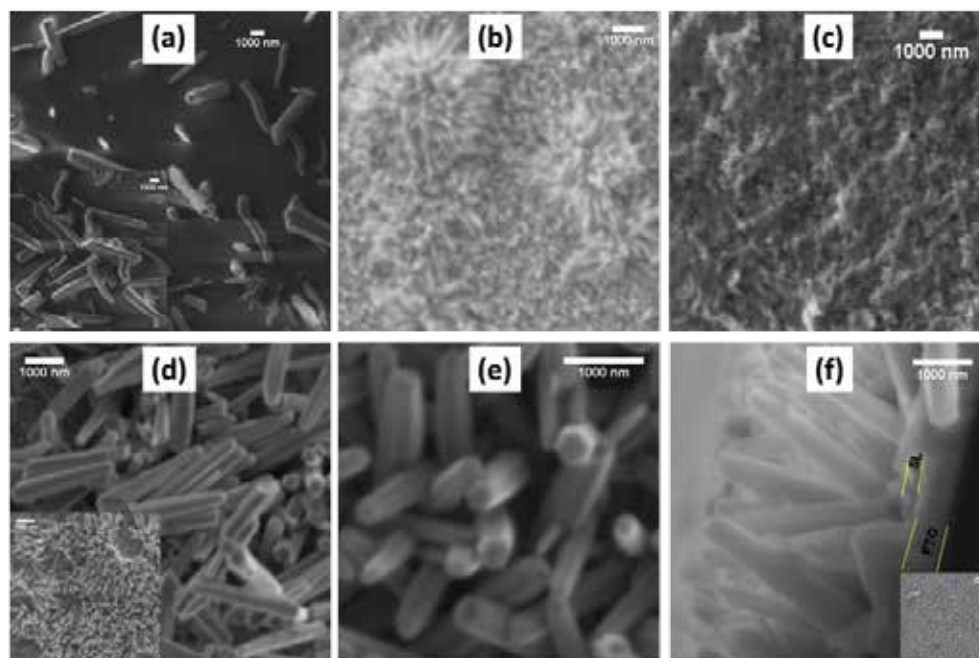
Fig. 4. SEM micrographs of ZnO NR/glass (a), ZnO NR/ZS/glass (b), ZnO Seed (ZS) layer/glass(c); ZnO NR/FTO (d), ZnO NR/ZS/FTO (e) and cross-sectional image of ZnO NR/ZS/FTO (f). The inset in (a) and (d) are the different location of the same sample; the inset in (f) is the blank FTO substrate

and collecting all data and all data were normalized to a reference sample as described in the characterization techniques section. The optical measurements of ZnO NRs grown on the seeded and non-seeded SLG and FTO substrates are shown in fig. 5 below. As can be seen from fig. 5(a,c), the near band absorption edge (dotted vertical lines) and a shoulder peak in the range 3.40 eV to 4.00 eV are indicating that ZnO has formed, but only a thin layer in the
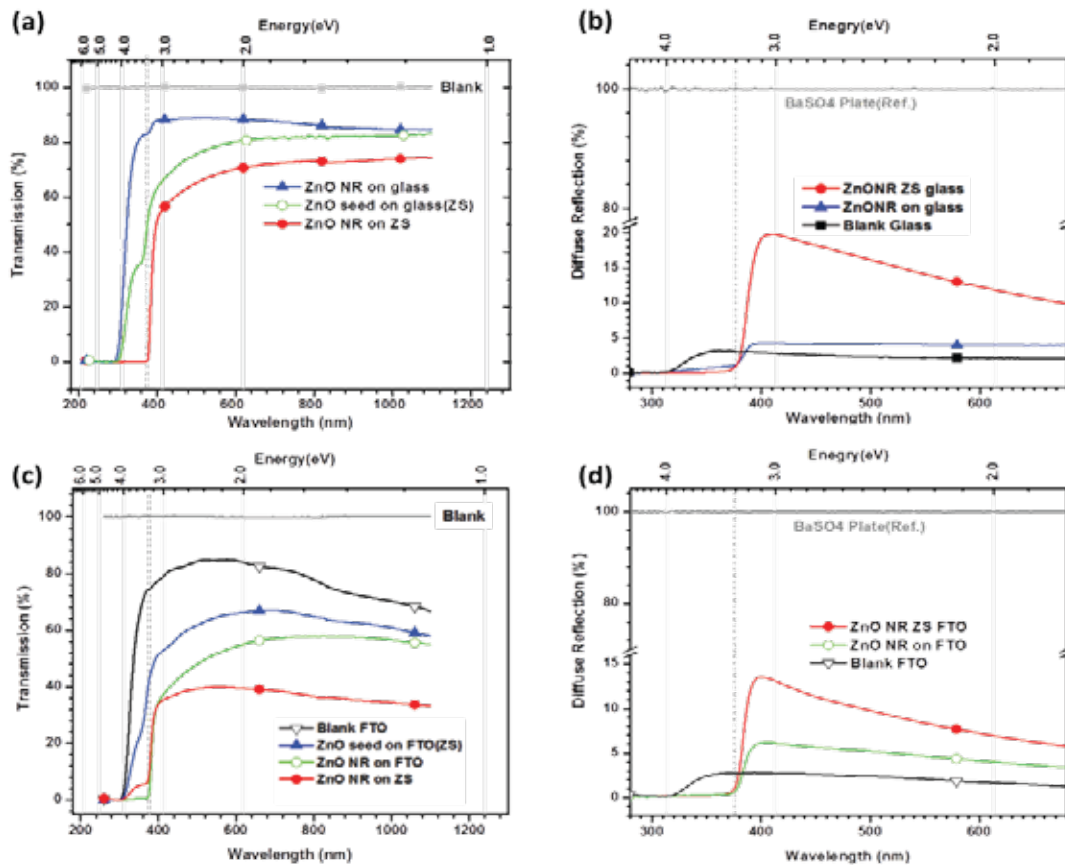
Fig. 5. Normalized Transmission and Diffuse reflection data of ZnO thin films grown on (a,b) glass substrate and (c,d) FTO substrate. Diffuse Reflection data of blank Glass and FTO substrates are also included in the respective panel for comparison purposes

concern samples. The normalized transmission through ZnO NRs is seen to be significantly reduced compared to ZnO seed (ZS) and blank substrates most probably scattering from the thicker film composed of ZnO NRs. This is in agreement with the normalized diffuse reflection data displayed in fig. 5(b,d), wherein ZnO NRs grown on seeded substrates exhibit enhanced reflection compared to those grown on non-seeded substrates. Therefore, optical analyses including SEM observations (see fig. 4) indicating that a pre-deposited ZnO seed promotes denser and thicker ZnO NRs films. The near band adsorption edge of ZnO nanostructures (denoted by dotted vertical lines in fig. 5(b,d)) in diffuse reflection spectra is consistent with that of transmission spectra and clearly distinguishable from the bare substrates.

Fig. 6 shows the Tauc plot generated from the diffuse reflection data of the ZnO NR samples, wherein data of ZS/SLG (in fig. 6(a)) and blank FTO (in fig.6 (b)) are also included for comparison purposes. From fig. 6(a), the

estimated bandgap for ZS/SLG, ZnO NR/SLG and ZnO NR/ZS/SLG were found to be ~3.27, ~3.20 and ~3.25 eV respectively. In contrast, the estimated band gap for ZnO NR/FTO, ZnO/ZS/FTO and blank FTO were found to be ~3.20 eV, ~3.25 eV and ~3.55 eV respectively (see fig. 6(b)).Notice that ZnO NRs grown on seeded and non-seeded substrates (both SLG and FTO) exhibit roughly the same optical bandgap (3.20 – 3.25 eV) and they are in good agreement with the reported bandgap of ZnO nanostructures (Kim *et al.,* 2005; Mekhnache *et al.,* 2011; Xu *et al.,* 2014). To supplement optical bandgap measurements of nanostructured ZnO film as well as to identify defect-related emission, PL measurements were also carried out and depicted in figure 7 below. Form the literature, most PL spectra of ZnO thin film (Çopuroğlu *et al.,* 2009; Kim *et al.,* 2005; Yefan Chen *et al.,* 1997) and ZnO NRs (Djuriię *et al.,* 2007; Sun and Ashfold, 2007; Sun *et al.,* 2006; Yin *et al.,* 2014) show both the 380 nm
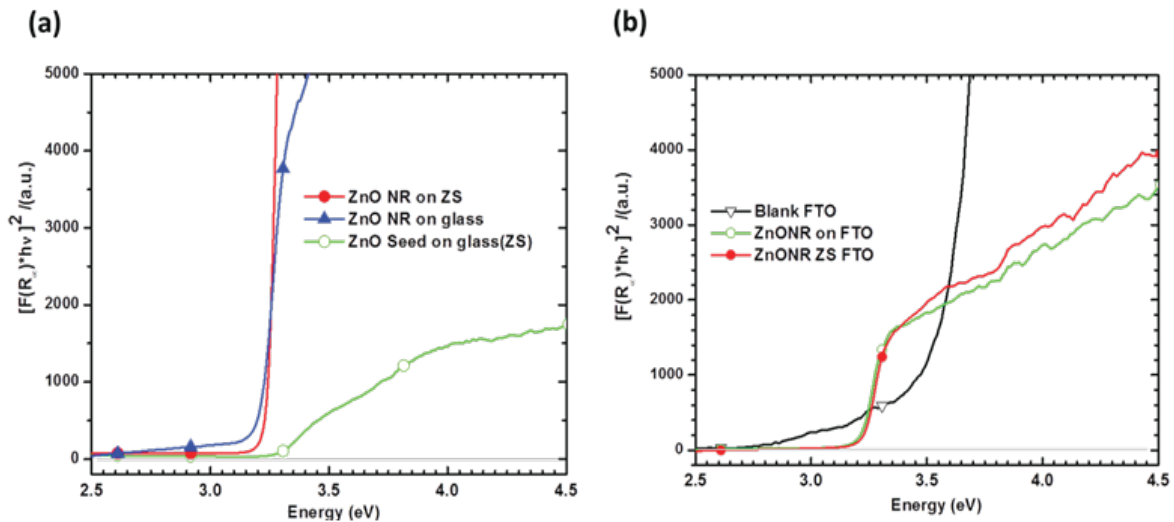
Fig. 6. Tauc plot for estimating band gap using diffuse reflection data of ZnO thin films grown on (a) SLG and (b) FTO substrate. Diffuse Reflection data of blank SLG and FTO substrates are also included in the respective panel for comparison purposes.
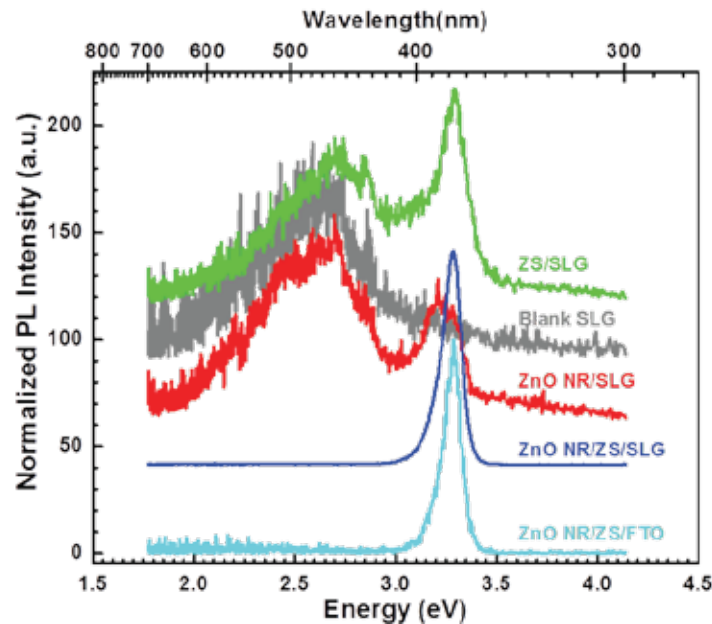

Fig. 7. Normalized PL spectra (vertically offset for clarity) of ZS and ZnO NRs films recorded at room temperature.The PL intensity is normalized with respect to the highest peak height for all samples. The broad peak at ~2.6 eV(~490 nm) in panel originates from underlying SLG substrate.

UV emission feature and a much broader emission feature in the visible region (500 – 600 nm) (Djuriię *et al.,* 2007). The luminescent peak centering at~380 nm has been attributed to the near-band-edge (NBE) transition of ZnO due to the recombination of free excitons, while the luminescent features in the visible region have been attributed to the various defects, such as oxygen vacancies (V_o), oxygen interstitials (O_i) and zinc interstitials (Zn_i) etc., present in the ZnO crystal lattice (Djuriię *et al.,* 2007; Sun and Ashfold, 2007). Therefore, one can assess the ZnO

product quality by simply estimating the ratio of the UV and Visible luminescent peak intensities (I_{uv}/I_{vis}) (Sun *et al.,* 2006).

In fig. 7 the PL spectra of a blank SLG substrate (gray curve) is compared and contrasted with that of ZS and ZnO NRs films.The broad emission feature centering at ~2.6 eV (~490 nm) in the PL spectra may originate from the underlying SLG substrate, as this feature is absent in the relatively thicker and dense ZnO NRs/ZS films produced on both SLG and FTO substrates (see also figure 3). Strikingly, all samples displayed a sharp near-band-edge (NBE) at ~378 nm (~3.25 eV) and barely detectable green-yellow emission peak (s) in the RT-PL spectra. This PL feature is indicating high crystalline quality of our chemical route synthesized ZnO NRs presumably with no or very low defect densities. In addition, the NBE value (~3.25 eV) from PL spectra is reasonably in good agreement with the estimated optical bandgap (~3.20 – 3.25 eV) of the ZnO NRs using diffuse reflection data. It is worth noting that both ZS and ZnO NR grown by facile chemical routes produced defect free good crystalline and optical quality materials. Defect-free well-aligned ZnO NR electrodes are desirable for ZnO/Cu_2O based optoelectronic device applications (Farhad, 2016; Farhad *et al.,* 2018). Further experimental investigations are currently in progress to confirm the presence of green-yellow defects in hydrothermally grown ZnO NRs with and without post-heat treatment in different ambient conditions and will be communicated elsewhere.

Conclusion

In this work, we have deposited both oriented ZnO seed and ZnO NRs by facile chemical routes on soda lime glass and FTO coated glass substrates. XRD analyses evidenced that the deposited films are highly *c*-axis textured. The SEM micrographs reveal that pre-depositing a ZnO seed layer is beneficial for growing aligned ZnO NRs along the *c*-axis direction parallel to the substrate normal. The optical bandgap of nanocrystalline ZnO seed and ZnO NRs estimated by the UV-VIS-NIR spectroscopy were found to be in the range 3.45 – 3.95 eV and 3.20 – 3.25 eV respectively and consistent with the reported results in the literature. The RT-PL analyses further confirmed that ZnO NRs grown on ZnO seeded glass are single crystalline like and free from defect-related green-yellow emission peaks.

Acknowledgement

Declarations of interest: We declare that we have no conflict of interest.

References

Ashfold MNR, Doherty RP, Ndifor-Angwafor NG, Riley DJ and Sun Y (2007), The kinetics of the hydrothermal growth of ZnO nanostructures, *Thin Solid Films,* **515**(24): 8679-8683. DOI: 10.1016/j.tsf.2007.03.122

Bao D, Gu H and Ku A (1998), Sol-gel-derived *c*-axis oriented ZnO thin films, *Thin Solid Films* **312**(1-2): 37-39. DOI: 10.1016/S0040-6090(97)00302-7

Baruah S and Dutta J (2009), Effect of seeded substrates on hydrothermally grown ZnO nanorods, *Journal of Sol-Gel Science and Technology* **50**(3): 456-464. DOI: 10.1016/S0040-6090(97)00302-7

Chen Y, Bagnall D and Yao T.(2000), ZnO as a novel photonic material for the UV region, *Materials Science and Engineering B* **75:** 190–198. DOI: 10.1016/ S0921-5107(00)00372-X

Çopuroğlu M, Koh LHK, O'Brien S and Crean GM (2009),Comparative characterisation of zinc oxide thin films prepared from zinc acetate with or without water of hydration via the sol–gel method, *Journal of Sol-Gel Science and Technology* **52**(3): 432-438. DOI: DOI: 10.1016/S0921-5107(00)00372-X

Djuriię AB, Leung YH, Tam KH, Hsu YF, Ding L, Ge WK and Phillips DL (2007), Defect emissions in ZnO nanostructures, *Nanotechnology* **18**(9): 095702. DOI: 10.1088/0957-4484/18/9/095702

Farhad, SFU (January 2016), Copper Oxide Thin Films grown by Pulsed Laser Deposition for Photovoltaic Applications, *PhD* Thesis, University of Bristol, UK, British Library EThOS. http://ethos.bl.uk/ Order Details. do?uin=uk.bl.ethos.691178

Farhad SFU, Richard FW and Cherns D (2018), Electron microscopy and diffraction studies of pulsed laser deposited cuprous oxide thin films grown at low substrate temperatures, Materialia 3: 230 - 238. DOI: 10.1016/j.mtla.2018.08.032.

Greene LE, Matt Law, Dawud H, Tan, Max Montano, Josh Goldberger, Gabor Somorjai and Yang P (2005), General Route to Vertical ZnO Nanowire Arrays Using Textured ZnO Seeds, *Nano Lett.* **5**(7): 1231-1236. DOI: 10.1021/nl050788p

Hiramatsu M, Imaeda K, Horio N and Nawata M (1998), Transparent conducting ZnO thin films prepared by XeCl excimer laser ablation, *Journal of Vacuum Science & Technology A: Vacuum, Surfaces, and Films* **16**(2): 669-673. DOI: 10.1116/1.581085

Huang MH, Mao S, Feick H, Yan H, Wu Y, Kind H and Yang P (2001), Room-Temperature Ultraviolet Nanowire Nanolasers, *Science* **292:** 1897-1899. DOI: 10.1126/science.1060367

Islam MR, Podder J, Farhad SFU and Saha DK (2011), Effect of Annealing on the Structural and Optical Properties of Nano Fiber ZnO Films Deposited by Spray Pyrolysis, *Sensors and Transducers Journal* **134**(11): 170-176.

Jeong H, Salas-Montiel R and Jeong MS (2015), Optimal length of ZnO nanorods for improving the light-extraction efficiency of blue InGaN light-emitting diodes, *Opt Express* **23**(18): 23195-23207. DOI: 10.1364/ OE.23. 023195

Kim JS, Marzouk HA, Reucroft PJ and Hamrin JCE (1992), Characterization of high quality c axis oriented ZnO thin films grown by metal organic chemical vapor deposition using zinc acetate as source material, *Thin Solid Films* **217:** 133-137. DOI: 10.1016/ 0040-6090(92)90619-M

Kim YS, Tai WP and Shu SJ (2005), Effect of preheating temperature on structural and optical properties of ZnO thin films by sol–gel process, *Thin Solid Films* **491**(1-2): 153-160. DOI: 10.1016/ 0040-6090(92)90619-M

Kumar M, Singh Bhati V, Ranwa S, Singh J and Kumar M (2017), Pd/ZnO nanorods based sensor for highly selective detection of extremely low concentration hydrogen, *Sci Rep.* **7**(1): 236. DOI: 10.1038/ s41598-017-00362-x

Mekhnache M, Drici A, Saad Hamideche L, Benzarouk H, Amara A, Cattin L and Guerioune M (2011),

Properties of ZnO thin films deposited on (glass, ITO and ZnO:Al) substrates, *Superlattices and Microstructures* **49**(5): 510-518. DOI: 10.1016/j.spmi.2011.02.002

Muth JF, Kolbas RM, Sharma AK, Oktyabrsky S and Narayan J (1999), Excitonic structure and absorption coefficient measurements of ZnO single crystal epitaxial films deposited by pulsed laser deposition, *Journal of Applied Physics* **85**(11): 7884-7887. DOI: 10.1063/1.370601

Nayeri FD, Soleimani EA and Salehi F (2013), Synthesis and characterization of ZnO nanowires grown on different seed layers: The application for dye-sensitized solar cells, *Renewable Energy* **60:** 246-255. DOI: 10.1016/ j.renene.2013.05.006

Peir AM, Ravirajan P, Govender K, Boyle DS, O'Brien P, Bradley DDC and Durrant JR (2006), Hybrid polymer/metal oxide solar cells based on ZnO columnar structures, *Journal of Materials Chemistry* **16**(21): 2088. DOI: 10.1039/ b602084d

Sarangi SNTA, Ray DK, Sahoo PK, Nozaki S, Sugiyama N and Uchida K (2017), ZnO-nanorods: A possible white LED phosphor. **1832**: 060022. DOI: 10.1063/1.4980427

Schmidt-Mende L and MacManus-Driscoll JL (2007), ZnO – nanostructures, defects and devices, *Materials Today* **10**(5): 40-48. DOI: 10.1016/s1369-7021(07)70078-0

Solís-Pomar F, Martínez E, Meléndrez MF and Pérez-Tijerina E (2011), Growth of vertically aligned ZnO nanorods using textured ZnO films, *Nanoscale Research Letters* **6:** 524. DOI: 10.1186/ 1556-276X-6-524

Sun Y and Ashfold MNR (2007), Photoluminescence from diameter-selected ZnO nanorod arrays, *Nanotechnology* **18**(24): 245701. DOI: 10.1088/0957-4484/18/24/245701

Sun Y, Fox NA, Riley DJ and Ashfold MNR (2008), Hydrothermal Growth of ZnO Nanorods Aligned Parallel to the Substrate Surface, *J. Phys. Chem. C.* **112:** 9234–9239. DOI: 10.1021/jp8019107

Sun Y, Fuge GM and Ashfold MN R (2006), Growth mechanisms for ZnO nanorods formed by pulsed laser deposition, *Superlattices and Microstructures* **39**(1-4): 33-40. DOI: 10.1021/jp8019107

Tan ST, Chen BJ, Sun XW, Fan WJ, Kwok HS, Zhang XH and Chua SJ (2005), Blueshift of optical band gap in ZnO thin films grown by metal-organic chemical-vapor deposition, *Journal of Applied Physics* **98**(1): 013505. DOI: 10.1063/1.1940137

Vayssieres L (2003), Growth of Arrayed Nanorods and Nanowires of ZnO from Aqueous Solutions, *Adv Mater* **15**(5): 464-466. DOI: 10.1002/adma.200390108

Xu J, Chen Z, Zapien JA, Lee CS and Zhang W (2014), Surface engineering of ZnO nanostructures for semiconductor-sensitized solar cells, *Adv Mater* **26**(31): 5337-5367. DOI: 10.1002/adma.200390108

Yefan Chen DM, Bagnall Ziqiang Zhu, Takashi Sekiuchi, Ki-tae Park and Kenji Hiraga and Goto T (1997), Growth of ZnO single crystal thin films on c-plane (0001) sapphire by plasma enhanced molecular beam epitaxy, *Journal of Crystal Growth* **181:** 165-169. DOI: 10.1016/S0022-0248(97)00286-8

Yin Y, Sun Y, Yu M, Liu X, Yang B, Liu D and Ashfold MNR (2014), Controlling the hydrothermal growth and the properties of ZnO nanorod arrays by pre-treating the seed layer, *RSC Adv.* **4**(84): 44452-44456. DOI: 10.1039/c4ra05008h

Zhang Z, Liao Q, Yu Y, Wang X and Zhang, Y (2014), Enhanced photoresponse of ZnO nanorods-based self-powered photodetector by piezotronic interface engineering, *Nano Energy* **9:** 237-244. DOI: 10.1016/j.nanoen.2014.07.019